Supplementary Information

Evaluation of Mn^{2+} sulfonylcalixarene complex- based materials for Oxygen Sensing

L. Bois*[,1], L. Mailler [1], T.Grange[1], G. Ledoux[2], E. Jeanneau[1], C. Desroches[1]

[1] Laboratoire des Multimatériaux et Interfaces, UMR CNRS 5615, 6, rue Victor Grignard, Université Lyon1-CNRS, 69622 Villeurbanne Cedex, France

[2] Institut Lumière Matière, UMR CNRS 5306, 10 Rue Ada Byron, Université Lyon1-CNRS, 69622 Villeurbanne Cedex, France

Table S1 : X-ray data of the Mn-KF-cryst (1), Mn-TBAF-cryst (2) and Mn-KF-DMF-cryst (3) after recrystallization of (1) in DMF .MeOH presence was clearly seen in the Mn-KF-cryst (1). DMF presence was highly suspected in Mn-KF-DMF-cryst (3).

	Cx KF (1)	**Cx TBAF (2)**	**Cx KF DMF (3)**
Formula	$C_{85.3}$ $H_{109.18}$ F K Mn_4 $O_{29.3}$ S_8	C_{96} H_{124} F Mn_4 N O_{24} S_8	C_{94} H_{124} F Mn_4 N_4 K O_{30} S_8
Space Group	P-1	C 2/m	P-1
Cell Lengths (Å)	**a** 12.1491 **b** 12.9634 **c** 17.3393	**a** 21.3377 **b** 13.4040 **c** 18.9593	**a** 14.12620 **b** 14.96940 **c** 15.85530
Cell Angles	α 72.172 β 81.666 γ 64.773	α 90.000 β 107.275 γ 90.000	α 116.2920 β 105.4010 γ 98.6590
Cell Volume	2351.42	5177.95	2754.96
Pore size (Å)	2.1 with solvent 4.1 without solvent	3.1 with solvent -	- 4.3 without solvent
Density	1.52	1.54	1.40
CCDC	824786	2034491	2516881

Table S2: Specific surface area (S), porous volume V_p, mesoporous volume V_{meso}, microporous volume V_{micro} (from t plot) and porous radius r_p from NLDFT, of the Mn-KF-cryst, Mn-KF-part, Mn-TBAF-cryst and Mn-TBAF-part.

Sample	**S (m^2/g)**	**V_p (cm^3/g)**	**V_{meso} (cm^3/g)**	**V_{micro} t plot (cm^3/g)**	**r_p NLDFT (nm)**
Mn-KF-cryst	65	0.08	0.03	0.01	0.98
Mn-TBAF-cryst	1	0.01	-	-	-
Mn-KF-part	221	0.36	0.16	0.03	1.11
Mn-TBAF-part	6	0.02	-	-	-

Table S3 : K_{sv} and k_q from the Lehrer models calculated from intensity curves and from the short time component of the decay curves. I_0/I_{air} and t_0, and t_0/t_{air} from the decay curves (short times).

Samples	K_{sv} $(I_0/\Delta I)$ kPa^{-1}	I_0/I_{air}	K_{sv} $(t_0/\Delta t)$ kPa^{-1}	t_0 (µs)	t_0/t_{air}	$k_{q\ from\ I}$ $[Pa^{-1}s^{-1}]$	$k_{q\ from\ t}$ $[Pa^{-1}s^{-1}]$
Mn-KF-part	2.40	28.1	0.42	150	3.9	16	2.8
Mn-KF-part-PIBMA	1.85	28.4	0.35	60	2.4	30.8	2.5
Mn-KF-part-PS	1.87	30.0	0.76	72	2.3	25.9	3.1.
Mn-TBAF-part	0.51	7.3	0.32	120	4.0	4.2	3.0
Mn-TBAF-part-PIBMA	0.67	14.1	0.35	110	2.7	6.1	3.2
Mn-TBAF-part-PS	0.52	13.4	0.55	172	3.6	3.0	3.2

Table S4 : Lifetime, K_{sv}, Stern-Volmer constant,. k_q quenching constant, $t_0/t_{air\ and}$ I_0/I_{air} and response time of some reference oxygen sensors.

Complex type	Lifetime (t_0) µs	K_{sv} (kPa^{-1})	k_q $[Pa^{-1}s^{-1}]$	t_0/t_{air}	I_0/I_{air}	Response time (ms)	Reference
Pd porphyrin	980	68	70	198	106	150	a
Pt porphyrin	71	4.2	59	80	13	250	a
Ru polypyridyl	5	1	-	1.4	2	variable	b
Ir complex	480	27	56	3		variable	c
Mn-KF-part	150	2.4	16	3.9	28.1		this work
Mn-TBAF-part	120	0.5	4.1	4.0	7.3	300	this work

References:

[a] Borisov, S. M.; Lehner, P.; Klimant, I. Novel Optical Trace Oxygen Sensors Based on Platinum(II) and Palladium(II) Complexes with 5,10,15,20-Meso-Tetrakis-(2,3,4,5,6-Pentafluorphenyl)-Porphyrin Covalently Immobilized on Silica-Gel Particles. *Analytica Chimica Acta* **2011**, *690* (1), 108–115. https://doi.org/10.1016/j.aca.2011.01.057.

[b] Wang, X.; Wolfbeis, O. S. Optical Methods for Sensing and Imaging Oxygen: Materials, Spectroscopies and Applications. *Chem. Soc. Rev.* **2014**, *43* (10), 3666–3761. https://doi.org/10.1039/C4CS00039K.

[c] Medina-Castillo, A. L.; Fernández-Sánchez, J. F.; Klein, C.; Nazeeruddin, M. K.; Segura-Carretero, A.; Fernández-Gutiérrez, A.; Graetzel, M.; Spichiger-Keller, U. E. Engineering of Efficient Phosphorescent Iridium Cationic Complex for Developing Oxygen-Sensitive Polymeric and Nanostructured Films. *Analyst* **2007**, *132* (9), 929. https://doi.org/10.1039/b702628e.

Movie S1: Movie of the sample Mn-TBAF-part in PIBMA placed inside the chamber of the linkam stage with a flow of nitrogen, at the beginning of the movie nitrogen is replaced by air.

Movie S2: Movie of the sample Mn-TBAF-part in PIBMA under air while a 2 L/min flow of N_2 getting out of a 4 mm diameter tubing is brought close to the sample and moved around.

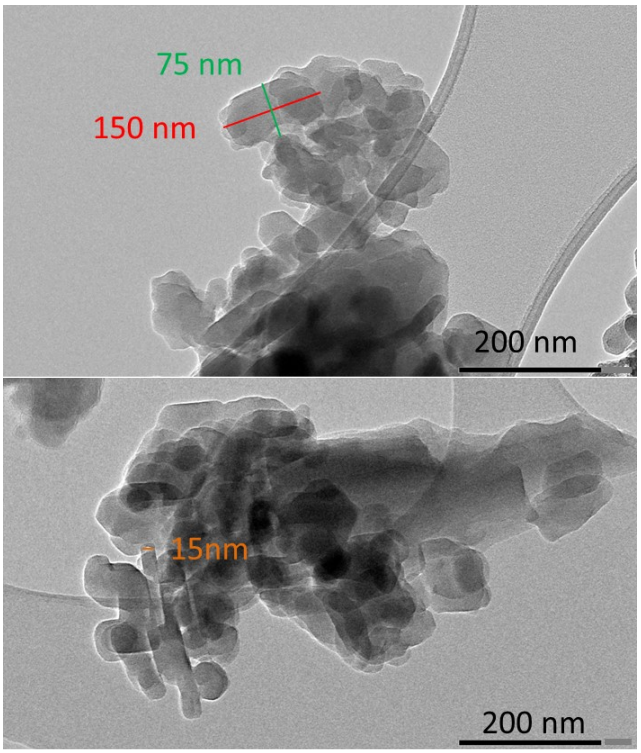

Fig. S1: TEM images of Mn-KF-part.

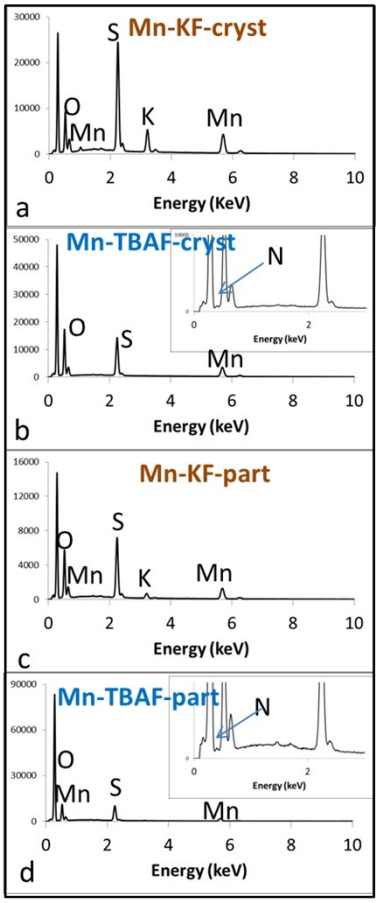

Fig. S2: EDS analysis of the Mn-KF-cryst (a), Mn-TBAF-cryst (b), Mn-KF-part (c) and Mn-TBAF-part (d).

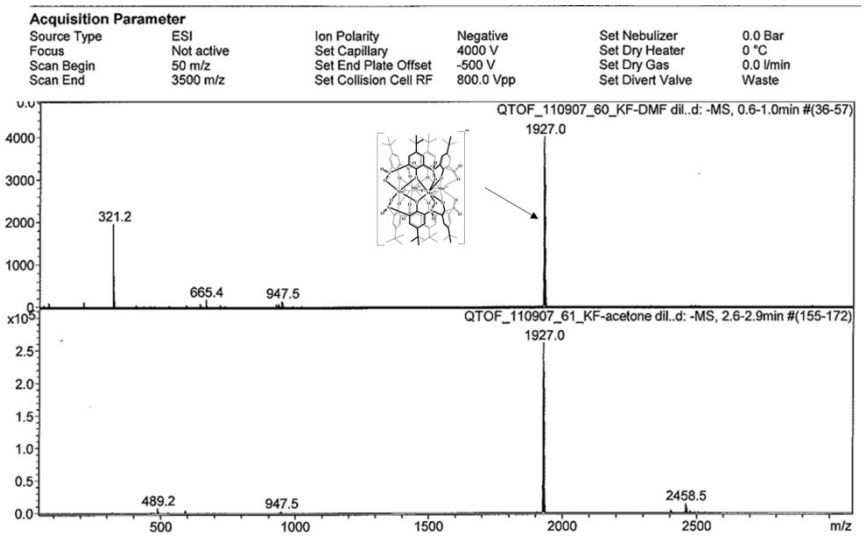

Fig. S3: Mass spectrometry of Mn-KF-part.

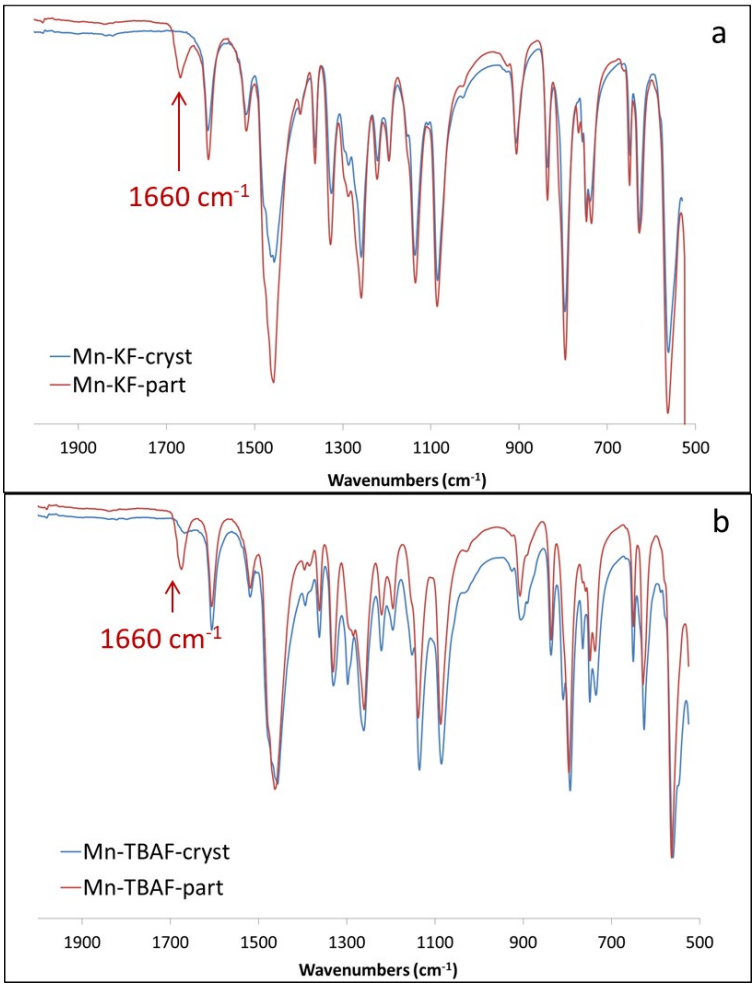

Fig. S4: FTIR spectra of the Mn- KF-cryst and Mn-KF-part (a) and Mn-TBAF-cryst and Mn-TBAF-part (b).

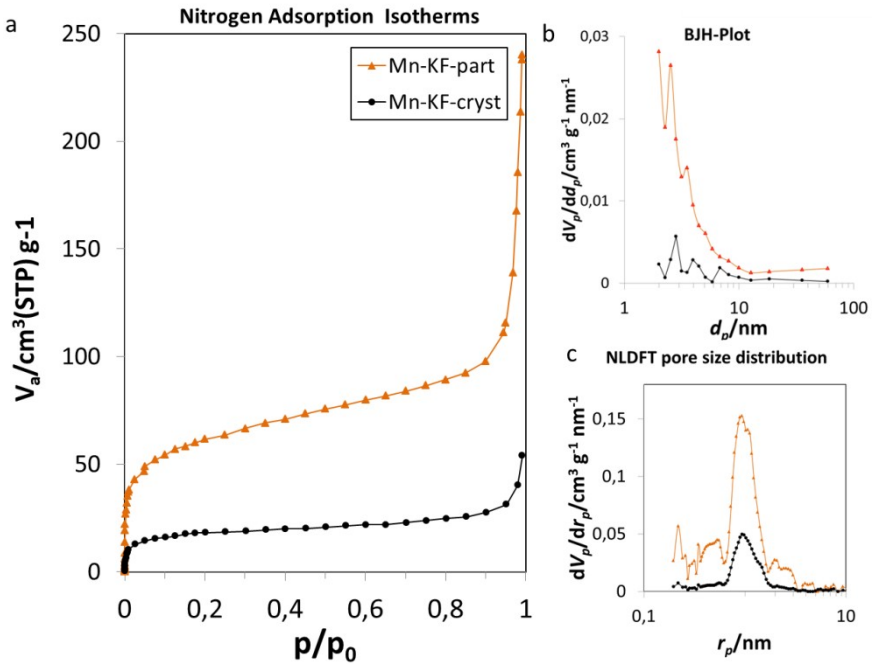

Fig. S5: Nitrogen Adsorption Isotherms (a), BJH pore size distribution (b) and NLDFT pore size distribution (c) of the Mn-KF-cryst and Mn-KF-part.

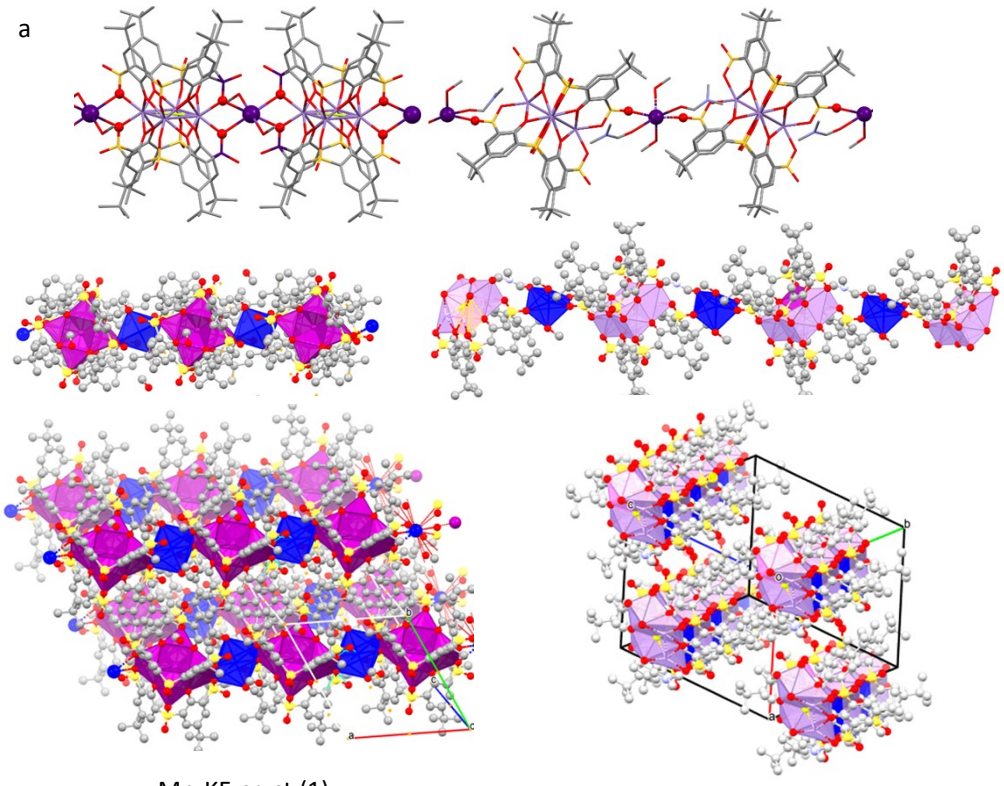

Fig. S6: Views of the packing of the Mn-KF complex (1): (a) and the Mn-KF-DMF complex (3): (b). F green, Mn purple, S yellow, O red, K blue, nitrogen blue, carbon grey).

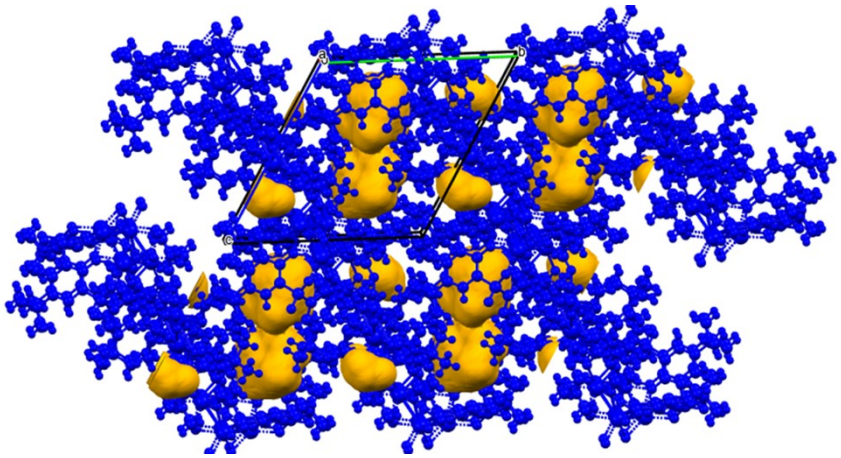

Mn-KF-DMF-cryst (3)

Fig. S7: Mercury contact surface visualization using probes of 1.2 Å in the Mn-KF-DMF complex (3)

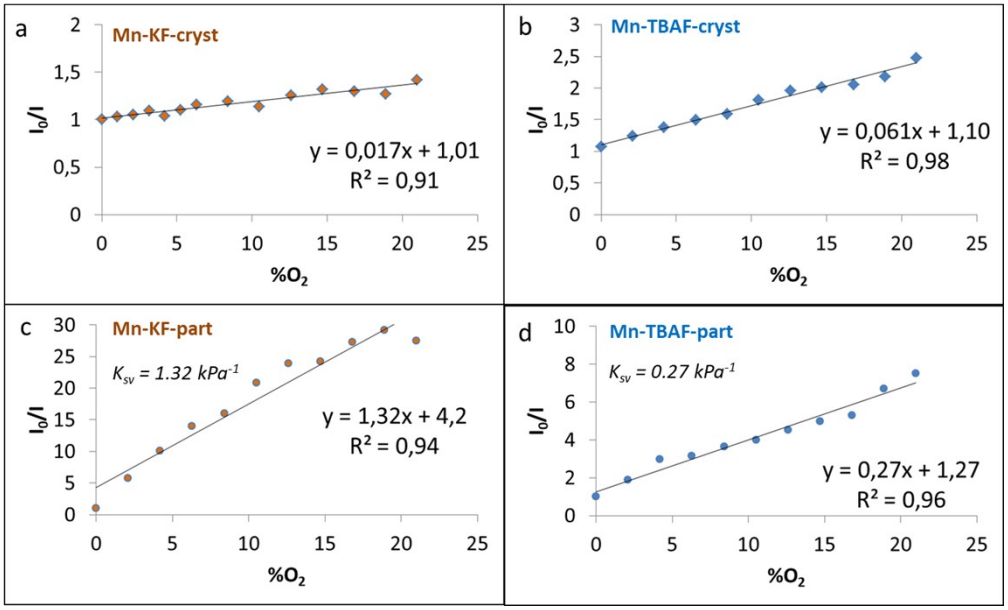

Fig. S8: Relative photoluminescence intensity curves versus $\%O_2$ of the Mn-KF-cryst (a), Mn-TBAF-cryst (b) Mn-KF-part (c) and of the Mn-TBAF-part (d) at different $O_2\%$.

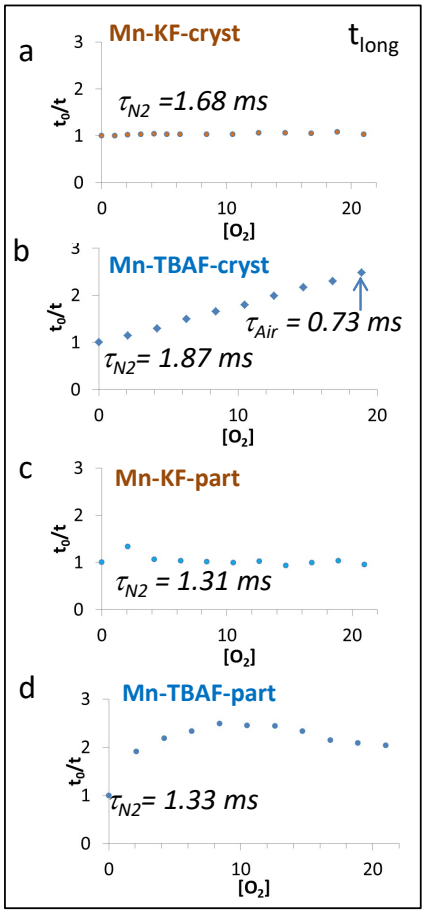

Fig. S9: Relative times of decay of the Mn-KF-cryst complex (a), Mn-KF-part (b), Mn-TBAF-cryst (c), and of the Mn-TBAF-part (d) at different O_2% in a temporal zones t_{long} between 0.6 and 2.6 ms.

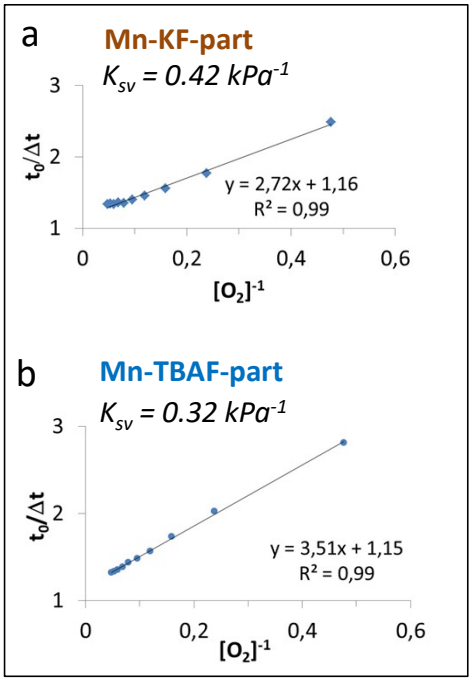

Fig. S10: Relative $t_0/\Delta t$ curves versus $[O_2]^{-1}$ of the Mn-KF-part (a) and Mn-TBAF-part (b) at different O_2%.

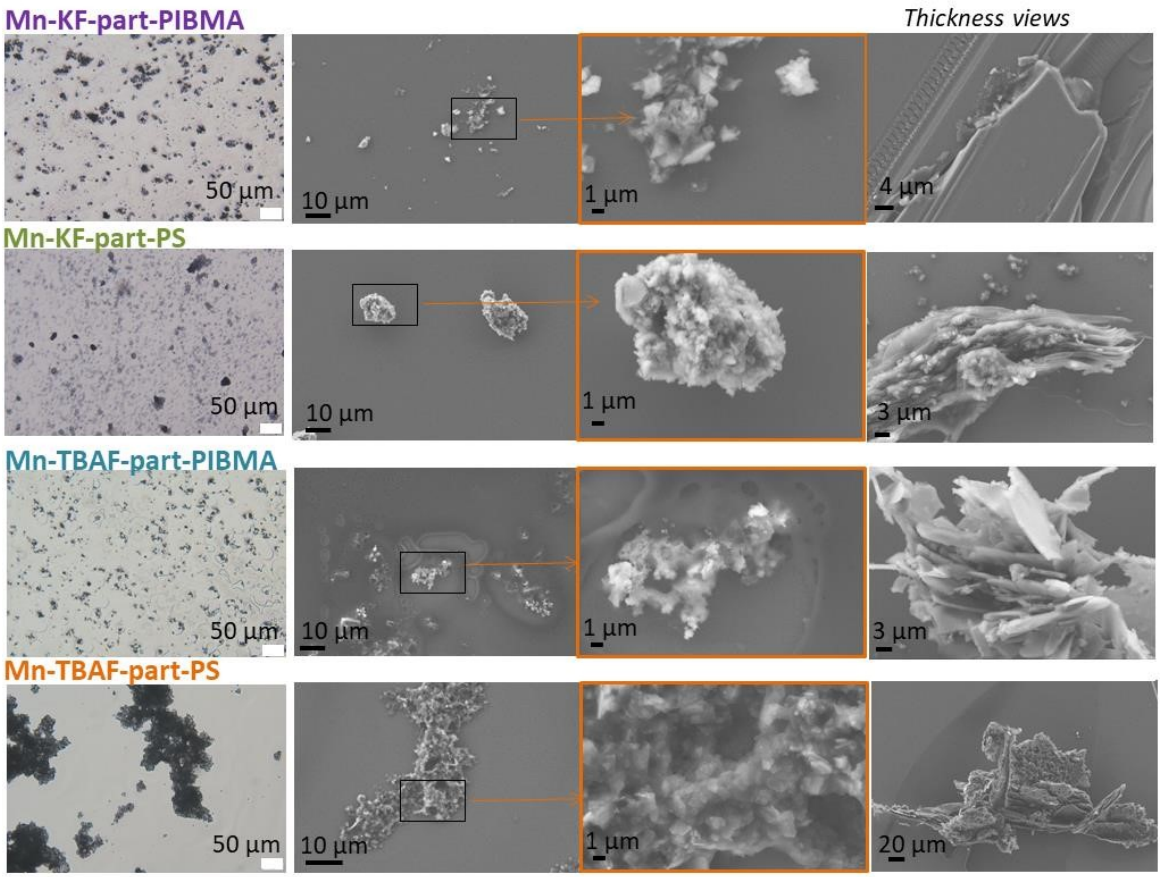

Fig. S11: Optical microscopy images (first row) of Mn-TBAF-part and Mn-KF-part in PIBMA and PS matrixes. SEM images of Mn-TBAF-part and Mn-KF-part in PIBMA and PS matrixes.(second row: global views; third row: detailed views; fourth row: thickness views after scraping with a razor).

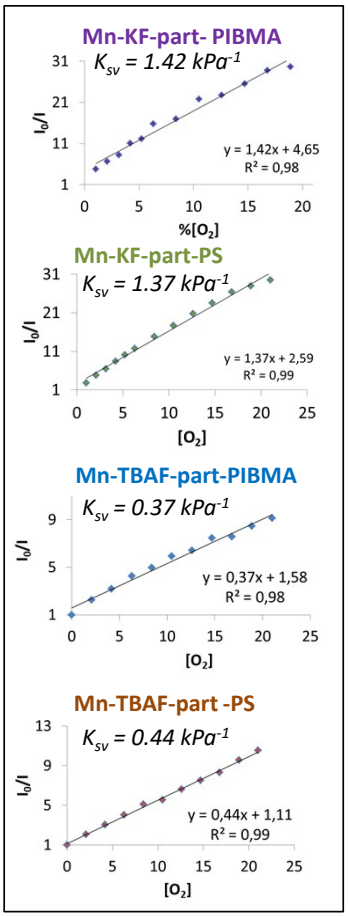

Fig. S12: Relative I_0/I curves versus $\%O_2$ of the Mn-TBAF-part and Mn-KF-part in PIBMA and PS matrixes at different $O_2\%$

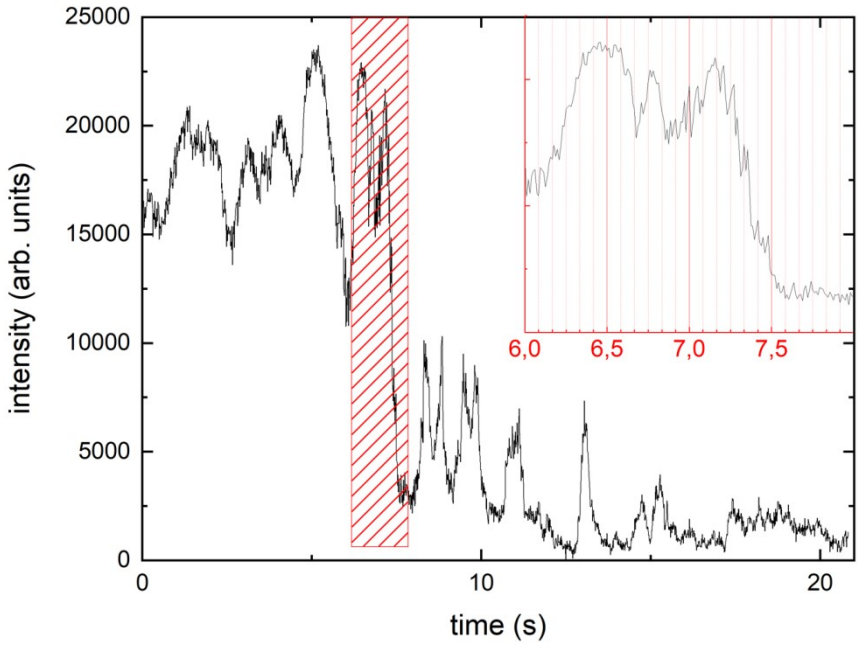

Fig. S13: Integration of a square of 5x 5 pixels from the movie of the sample Mn-TBAF-part in PIBMA with a flow of nitrogen, at the beginning of the movie nitrogen is replaced by air.